Granular Jamming as Controllable Stiffness Mechanism for Endoscopic and Catheter Applications

Loïc BLANC[1,*], Bertrand FRANÇOIS[2], Alain DELCHAMBRE[1], Pierre LAMBERT[1]

1. Université Libre de Bruxelles (BEAMS Department, CP 165/56) - 50 Av. FD Roosevelt - B-1050 Brussels, Belgium
2. Université Libre de Bruxelles (BATir Department, CP 194/2) - 50 Av. FD Roosevelt - B-1050 Brussels, Belgium

∗. loic.blanc@ulb.ac.be

Abstract

In the medical field, many tools have to be sufficiently flexible to follow the human body natural paths but stiff enough to transmit force. This dual requirement in stiffness can be solved with smart medical devices able to tune the stiffness of flexible tubes. In this work, the Granular Jamming solution is proposed to change flexible tube rigidity, by applying a pressure difference across a membrane. The solution is based on glass beads packed in a waterproof latex membrane. The device is flexible if the pressure difference is low, while it is more rigid when this pressure difference is increased. The contribution of this paper is a full characterization of the Granular Jamming solution for several granular materials and pressure differences. Triaxial compression tests give the equivalent compression Young modulus (E_c), while three-point bending tests provide a flexural stiffness (E_bI) from which an equivalent bending Young modulus (E_b) is deduced. The grain size has low influence on the Young modulus while the pressure difference has a large impact on the results both in compression and in bending. In the bending tests, a smaller diameter of the flexible tubes filled with the granular media leads to the largest equivalent bending Young modulus. As already reported, the Granular Jamming solution gives a significant change in flexural rigidity. Miniaturized solutions and bending models have to be further studied.

Key-words: Granular Jamming / Controllable stiffness / Bending test / Triaxial compression test / Medical devices.

Nomenclature

Parameter	Units	Definition
D	mm	Tube diameter
$\bar{d}$	mm	Mean diameter of the glass beads
E_b	MPa	Equivalent Young Modulus of the specimens in bending
E_bI	Nmm^2	Flexural stiffness of the specimens
E_c	MPa	Equivalent Young Modulus of the specimens in compression
E_g	GPa	Young Modulus of the glass beads
F_c	N	Force applied on the specimen in compression
F_b	N	Force applied on the specimen in bending
I	mm^2	Second moment of area of the specimen
L	mm	Length of the specimen
L_s	mm	Support span length in three-point bending test
n	none	Exponential coefficient in exponential law
P_1	kPa	Pressure in the specimen
P_2	kPa	Pressure of the surrounding environment
P_{atm}	kPa	Atmospheric pressure
p'	MPa	Mean effective stress
q	MPa	Deviatoric stress
q_u	MPa	Deviatoric stress at failure
t	mm	Thickness of the membrane
α	none	Stiffness gain between rigid and flexible states
ΔP	kPa	Pressure difference across the membrane
δ	mm	Deflection measured during the bending test
ϵ	none	New strain after correction of starting of triaxial compression test
$\epsilon*$	none	Strain of triaxial compression test in initial conditions
σ_1	MPa	Longitudinal or axial principal stress
σ_2	MPa	Lateral principal stress
σ_3	MPa	Radial principal stress

1 Introduction

The vascular occlusion, one of the widespread cardiovascular diseases, is a reduction of the cross-section of a blood vessel. One of the possible interventions for removing this occlusion is the appositioning of a stent. In order to treat vascular stenosis by stenting, a guidewire has to pass through the occlusion such that a balloon catheter can deliver the stent at the right location [1]. In this case, the guidewire has to be flexible to reach the stenosis after having followed a possible tortuous path through the blood vessels. Once it has reached the stenosis, it requires a rigid support to pass through the occlusion for treatment, to avoid buckling or deformation due to the force application. During treatment of chronic total occlusions, 63% of the procedural failures are due to the inability of the guidewires to cross the occlusion [2].

During minimally invasive procedures, most of the devices (endoscopes, catheters, guidewires, etc.) need to be sufficiently flexible to avoid damaging patient tissues or causing pain, but have to be stiff enough to transmit force (e.g. to support other tools or to puncture tissues [3]). These needs can be found in laparoscopic, endoscopic, gastro-enterologic and cardio-vascular interventions. In order to solve this duality on the rigidity, various controllable stiffness mechanisms have been proposed [4, 5, 6, 7, 8, 9, 10, 11, 12, 13, 14].

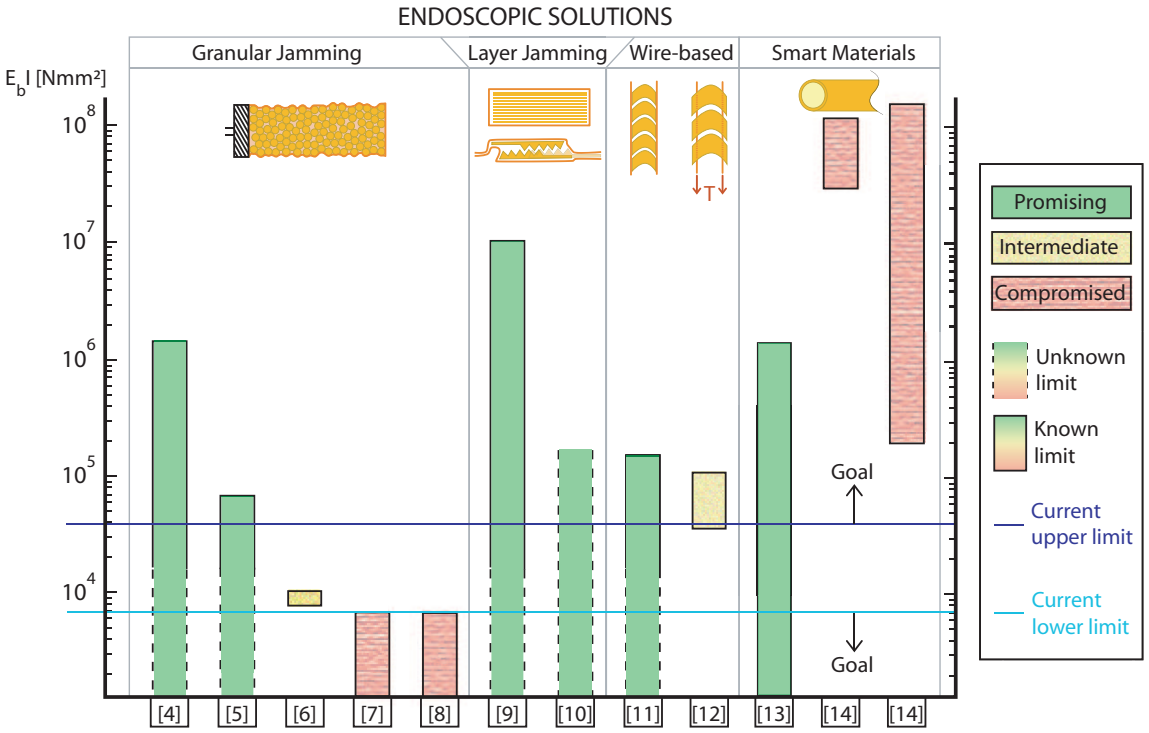

Figure 1: *Equivalent flexural rigidity (E_bI) for variable stiffness endoscopic solutions described in the literature. The current upper limit corresponds to the stiffest endoscope on the market. The current lower limit corresponds to pediatric endoscopes. Several other solutions exist, but have not been quantified.*

Figure 1 gives a quantitative comparison of most relevant solutions for variable stiffness and shape-locking solutions. Currently, most of the endoscopes have a fixed stiffness. In this figure,

the maximal limit corresponds to the stiffest endoscope currently available on the market [15], and the minimal limit corresponds to the stiffness of pediatric endoscopes [15]. The goal is therefore to have a flexible state more flexible than a pediatric endoscope and a rigid state more rigid than the stiffest endoscope. With this target, the controllable stiffness endoscope would have a larger range than the endoscopes on the market for now. The Granular Jamming is based on the locking of granular material, while Layer Jamming uses locking of layers. The wire-based solutions use locking of wires or tensions in wires to lock the device in a given configuration. The smart materials solutions are based on shape memory polymers, alloys and composites.

Variable stiffness mechanisms can be applied to other fields as for instance in robotics with the development of a robotic foot [16], in adaptative vibrations damping [17] and in bio-engineering for developing extracellular matrix [18]. This work focuses on endoscopic solutions with controllable stiffness and shape-locking effect. One of the promising solutions to achieve this objective and still open to various research questions is based on Granular Jamming [5]. In this study, the samples are composed of a flexible and waterproof membrane (1) filled with a specific granular material (glass microspheres (2)) as shown in Figure 2. The stiffness of the sample is related to the pressure difference across the membrane given by

$$\Delta P = P_2 - P_1, \tag{1}$$

where P_2 is the pressure corresponding to the surrounding environment and P_1 is the pressure observed inside the sample (in the membrane). If suction in the specimen is used to create the pressure difference, a filter (3) is required.

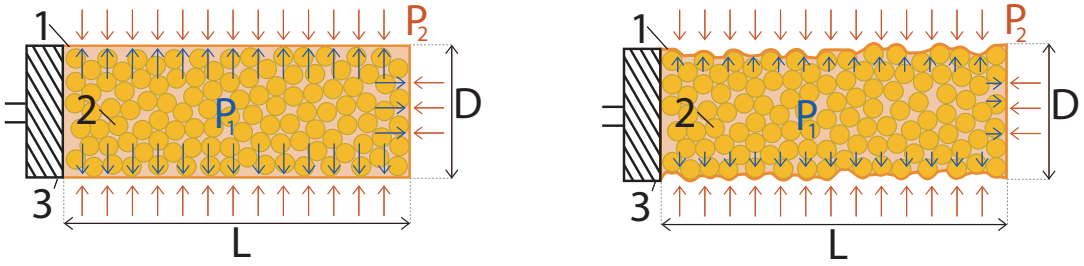

(a) *Flexible state* **(b)** *Rigid state*

Figure 2: *Granular Jamming enables the change of stiffness by modifying the pressure difference $\Delta P = P_2 - P_1$. (a) For low ΔP, the specimen is flexible. (b) For large ΔP, the specimen is rigid. D is the tube diameter and L the tube length. 1) Membrane; 2) Granular material; 3) Filter.*

When the pressure difference is low (the pressure in the sample is close to the pressure of the surrounding environment), the grains are free to move with respect to each other (Figure 2a). In this configuration, the system is flexible [19]. When the pressure difference is increased, the system is more rigid as the grains start to be locked to each other (Figure 2b). A fluidic control of the pressure difference across the membrane allows for adjusting the stiffness of the sample.

The Granular Jamming principle based on suction is suitable for medical applications as in case

of failure of the vacuum source, the system is flexible. It is therefore possible to remove easily the device in case of problem during the intervention. Furthermore, the use of suction is less dangerous than a source of high pressure in the human body.

This research aims at scaling such solutions down to $2.8\,\mathrm{mm}$ diameters, while current endoscopic solutions reported in the literature target the range from $15\,\mathrm{mm}$ to $22\,\mathrm{mm}$. Therefore, scaling laws must be integrated and the optimization of this solution must vary many influencing parameters.

2 Materials and Methods

The Granular Jamming solution can be characterized by two different mechanical testing methods. On the one hand, the triaxial compression test is routinely used in geomechanics to characterize the granular material itself in shearing conditions for various grain sizes and pressure differences. On the other hand, the three-point bending tests are performed in order to characterize the samples in a configuration closer to the final embodiment with several granular materials for different pressure differences.

2.1 Triaxial Compression Test

The triaxial compression test is used in geomechanics to characterize soils and granular materials under a defined confinement [20]. Triaxial tests permit to characterize the axial properties (stiffness and ultimate stress) under non-isotropic loading thanks to an isotropic pressure applied by pressurized water which is superimposed on the axial stress. This test allows for characterizing soils in conditions closer to the field. As shown in Figure 3, a sample (1) (granular material in a membrane (2)) is placed in the so-called triaxial cell (3) filled with water. The cell is placed on a loading frame equipped with an axial force sensor outside the cell. The mechanical connection bewteen the sample and the sensor (4) therefore induces friction forces in the sealing which have been measured to be negligible compared to the range of forces measured. The principal stresses can be controlled in the axial and radial directions (the triaxial test is cylindrical). The cylindrical sample has a length L approximately twice its diameter D. This ratio is used to ensure a proper observation of shearing [21].

The radial stress σ_3 is set by the confining pressure, fixed by a pressure controller and defined for each test. The longitudinal or axial stress σ_1 is equal to the sum of the confining pressure and the increasing longitudinal stress applied during the compression. The deviatoric stress q is defined in Equation 2 as the difference between the total longitudinal stress σ_1 and the radial stress σ_3 corresponding to the confinement [22].

$$q = \sigma_1 - \sigma_3 \tag{2}$$

A waterproof and elastic membrane of latex with diameter $D = 35\,\mathrm{mm}$ and thickness $t = 0.070\,\mathrm{mm}$ is used to separate the dry granular material contained by the sample from the con-

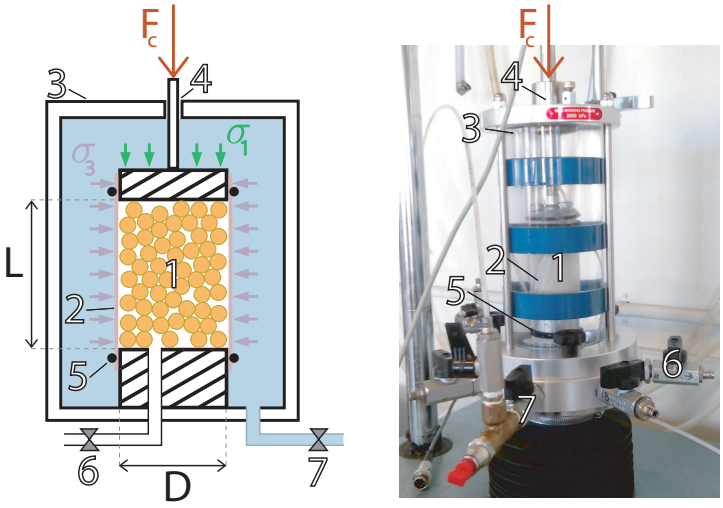

Figure 3: *Triaxial compression test set-up. D is the tube diameter, L the tube length, F_c the compression force, σ_1 the longitudinal stress and σ_3 the radial stress. 1) Triaxial test specimen; 2) Membrane; 3) Triaxial cell; 4) Mechanical connection between loading frame and specimen; 5) O-rings; 6) Drainage valve; 7) Cell valve.*

fining water filling the cell. A constant weight of glass beads is used in each specimen, ensuring a length of $L \approx 70\,\mathrm{mm}$ (the bulk density is very similar for each class of glass beads as seen in Table 1). The sealing of the sample is ensured by o-rings (5). The length L and diameter D of each specimen is measured for the stress-strain calculations to adjust the low variation in sample dimensions. In order to have a defined, repetitive and ideal cylindrical shape of specimen, a two-part mold is used to keep the sample under the form of a cylinder. As dry granular material (e.g. sand or glass beads) has no cohesion, the sample does not keep its shape due to gravity. Vacuum is therefore applied via the drainage valve (6) to the sample to solidify it (by using the principle of Granular Jamming) so that it remains in a well defined cylinder for the compression test. The specimen is placed in the triaxial cell and the confining pressure is applied via the cell valve (7), to reach the defined conditions of the test. Once the confining pressure is reached in the cell, the drainage valve is open to remove the vacuum in the sample and ensure that atmospheric pressure is set. Thanks to this procedure, a constant pressure difference is applied during the whole compression test (imposed by the confining pressure).

The triaxial compression tests can be drained (water inflow in the sample - remember that the confining water is separated from the granular material) or undrained (no water inflow in the sample) and consolidated (by confining pressure) or not (by quick application of loads). The drainage is ensured by the opening of a valve and a connection to a pressure controller. In this study, dry granular material is characterized. Therefore, only consolidated and quasi-static (with low strain rate) tests are performed with a drainage valve open to ambient air conditions to ensure a constant atmospheric pressure in the specimen. The strain rate is set to $0.35\,\mathrm{mms}^{-1}$. This strain rate has been determined during the preliminary study and validation step of the procedure for quasi-static tests, using dry sand of well known characteristics.

2.2 Three-Point Bending Test

There exist different ways to measure the flexural stiffness given by E_bI. The cantilever beam bending test and the three-point bending test are used to induce a bending in the sample by application of a static force as shown in Figure 4. The measurement of the bending force F_b and the displacement δ can be converted into the measurement of the flexural stiffness E_bI, knowing the length between the supports L_s:

$$E_bI = \frac{F_bL_s^3}{a\delta}, \tag{3}$$

where a is a constant ($a = 3$ for cantilever beam bending test and $a = 48$ for three-point bending test).

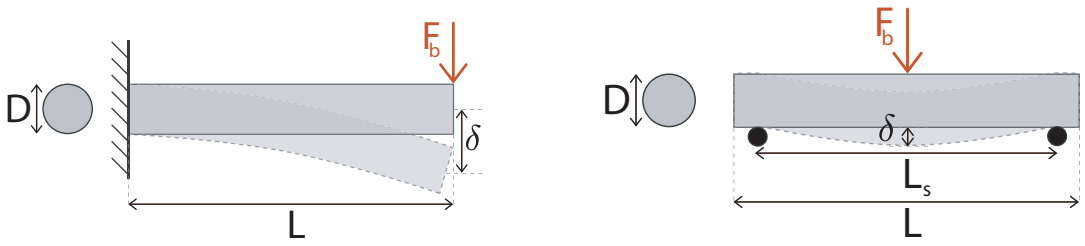

(a) *Cantilever beam bending test* **(b)** *Three-point bending test*

Figure 4: *Flexural stiffness can be calculated from cantilever beam and three-point bending tests. D is the tube diameter, L the tube length, δ the deflection, F_b the bending force and L_s the support span length for the three-point bending test.*

In [5, 7, 23], the main test to evaluate the performance of their Granular Jamming solution is the cantilever beam bending test. In [15], three-point bending test is used to measure the flexural stiffness of endoscopes. In [24], the authors propose to compare several methods and use the properties of buckling. Using material strength theory, the buckling threshold can be linked to the flexural stiffness. Other solutions to measure the flexural stiffness E_bI, can be performed in a dynamic regime [25].

In this study, the performances of the Granular Jamming solution are quantified by a three-point bending test. The samples are cylindrical with two possible diameters ($D = 15\,\mathrm{mm}$ and $D = 20\,\mathrm{mm}$), for a fixed length of $L = 200\,\mathrm{mm}$. This test bench is adapted to different sizes as the span length L_s can easily be adjusted. For these specimens, a span length of $L_s = 120\,\mathrm{mm}$ has been used. In the standardized three-point bending test [26], the length of the sample should be sufficiently larger than the sectional dimensions. Furthermore, the sample length should be larger than the span length to ensure that it exceeds the supports.

A natural rubber membrane, with a thickness of $t = 0.3\,\mathrm{mm}$, is used for these tests. The glass beads fill the membrane to the desired length $L = 200\,\mathrm{mm}$. The extremities of the specimens are 3D printed caps with an Objet Eden260VS from *Stratasys*. O-rings are used to ensure a good sealing between the membrane and the caps of the specimens. On one side, the cap has an hose tail for vacuum pump connection, on the other side, the cap is plain to ensure the

vacuum in the sample. The vacuum pump is a VCP 130 from *VWR International*. This pump is constantly connected and turned on during each test to ensure a constant vacuum in the specimen during the bending test. This vacuum is controlled with an IRV20 vacuum regulator from *SMC Pneumatics*.

In order to remove the influence of the weight of the specimen in the measurement of the flexural stiffness, the slope of the force-displacement curve is used instead of the absolute force obtained at a given displacement. This definition of stiffness removes the need of absolute values which improve the results of stiffness as no force or displacement offset could disturb the measurement. This allows for calculating the stiffness more precisely in the linear regime and differentiating the elastic and plastic phases. In this work, only the elastic regime is observed as no or very low strain losses are desired for medical applications. Absolute values at a given displacement are used in [5] to estimate the performance of the solution, while a range of forces is considered in [7], but the plastic deformation is not considered.

2.3 Granular Material

The granular materials used in this study are grinding materials, purchased at *Sigmund Lindner GmbH*. These beads are polydisperse, polished and made of soda lime glass with a specific weigth of $2.5\,\mathrm{kgl}^{-1}$. The Young modulus of these glass beads is $E_g = 63\,\mathrm{GPa}$. Five different mixes of glass beads are studied, with sub-millimetric diameters. Their characteristics are given in Table 1. The final goal targeted by this study is to obtain variable stiffness catheters or guidewires. This means that the diameter of the solution should not exceed $2.8\,\mathrm{mm}$ corresponding to the operating channel of classically used endoscopes [27]. Too large grains are therefore excluded. The sphericity of the glass beads has been chosen to simplify the interpretation of the results and to ease the development of a general model. The roundness used in Table 1 is defined by the ratio of the width (smallest dimension in the cross-section) over the length (largest dimension in the cross-section). However, spherical particles does not guarantee the highest stiffness obtained by Granular Jamming. In [5, 28], the edgy particles are giving better results in terms of stiffness. It is assumed that the flexible state is also impacted by this type of particles as the particles lock better to each other.

Table 1: *Glass beads characteristics from Sigmund Lindner GmbH*

Class	Article	Diameters	Mean diameter $\bar{d}$	Roundness	Bulk density
A	5214-7	$0.100 - 0.200\,\mathrm{mm}$	$0.170\,\mathrm{mm}$	≥ 0.89	$1.42\,\mathrm{kgl}^{-1}$
B	5216-7	$0.200 - 0.300\,\mathrm{mm}$	$0.255\,\mathrm{mm}$	≥ 0.89	$1.44\,\mathrm{kgl}^{-1}$
C	5223-7	$0.300 - 0.400\,\mathrm{mm}$	$0.341\,\mathrm{mm}$	≥ 0.89	$1.46\,\mathrm{kgl}^{-1}$
D	4502	$0.500 - 0.750\,\mathrm{mm}$	$0.684\,\mathrm{mm}$	≥ 0.95	$1.49\,\mathrm{kgl}^{-1}$
E	4503	$0.750 - 1.000\,\mathrm{mm}$	$0.941\,\mathrm{mm}$	≥ 0.95	$1.50\,\mathrm{kgl}^{-1}$

3 Results

In this section the results obtained by the previously described test benches are presented.

3.1 Triaxial Compression Test

The triaxial compression tests have been performed for all the different glass beads summarized in Table 1. Four different confining pressures have been used. These confining pressures correspond to pressure difference of half the atmospheric pressure ($\Delta P = 50.5\,\mathrm{kPa}$), atmospheric pressure ($\Delta P = 101\,\mathrm{kPa}$), two and four times the atmospheric pressure ($\Delta P = 202\,\mathrm{kPa}$ and $\Delta P = 404\,\mathrm{kPa}$). Using pressurized water for confinement allows for overpassing the limit of the atmospheric pressure encountered in the three-point bending test for which vacuum in the specimens is applied (as the surrounding environment cannot be controlled). The tests have been repeated three times for each confining pressure ΔP and each type of glass beads. The first test is a compression test until the specimen failure. It is used to determined the ultimate force in compression for the testing conditions. It has been observed that the initial conditions (packing of particles, contact forces of loading frame, dry friction, etc.) influences the beginning of the loading curve, which prevents a repeatable measurement of the Young modulus. Therefore, a specific procedure is applied for the two last tests in order to evaluate an equivalent Young modulus in compression E_c. The specimen is loaded up to 85% of the ultimate force observed in the first test. Then, the specimen is unloaded (reverse displacement of the loading frame), until the force drops to $F_c \approx 0\,\mathrm{N}$. Finally, a complete compression test is started again up to the failure of the specimen that ends up the test. Thanks to this cycling procedure, the initial conditions of the triaxial test are not influencing the calculation of the Young modulus E_c any more as it is calculated after the cycling phase only.

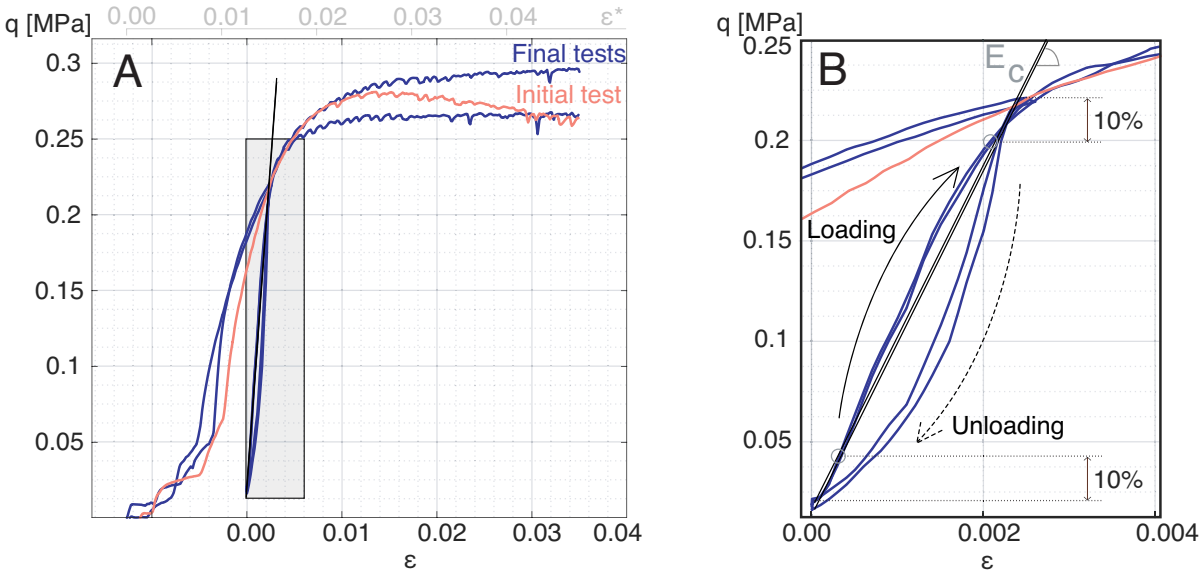

Figure 5: *(A) Deviatoric stress evolution for new equivalent strain with cycling procedure for class C glass beads at $P = 101\,\mathrm{kPa}$. The failure is measured at $q_u \approx 0.280\,\mathrm{MPa}$. The new strain ϵ is set to zero at the beginning of the second loading phase. The initial strain ϵ^* starts at the beginning of the triaxial compression test. (B) Zoomed-in of highlighted data in (A). A 10% margin on the stress is chosen for the linear regression over the new loading curve. The slope of the regression gives the compression Young modulus E_c.*

In Figure 5, stress-strain curves from these triaxial compression tests are drawn for class C

glass beads (cfr. Table 1) at $\Delta P = 101\,\mathrm{kPa}$. The deviatoric stress q is preferred as it does not count for the value of the confining pressure. The initial test giving the ultimate stress and the two repetitions of the tests with the cycling procedure are presented in this figure. The cycling phase ensures a better linear behavior. An equivalent Young modulus E_c can be calculated from this new loading phase. In this study, the Young modulus E_c is calculated on the new and more repetitive loading curve on which a linear regression is calculated. The slope of this linear regression gives the equivalent Young modulus in compression E_c of the specimen. A 10% margin around the limits of the loading curve, as shown in Figure 5, are chosen to ensure repetitive and linear results. The values of Young modulus E_c obtained by this method are more repetitive than based on the simple triaxial compression test because of the chaotic initial behavior [28]. The initial strain ϵ^* starts at the beginning of the triaxial test. The new strain ϵ starts after the cycling procedure.

The different confining pressures give different stress-strain curves. Figure 6 shows the strong dependence of the curve with the pressure difference obtained by the confining pressure. In this figure, the new loading curve after the cycling is represented with the new strain ϵ. The ultimate load increases with the pressure difference. The equivalent Young modulus in compression E_c (calculated on the linear regression slope) is also increasing.

Figure 7 represents the evolution of the equivalent Young modulus in compression E_c for the various glass beads that have been tested and for the different confining pressures in the triaxial compression tests. In the lower range of confining pressures (up to $101\,\mathrm{kPa}$), the behavior can be assumed to be linear. It actually follows an exponential law if larger confining pressures are used in the calculation. Hicher and Rahma [29] proposed a model for the Young modulus in compression E_c of specimen filled with glass beads based on Hertz's relation of contact between the spheres and their initial configuration. Simplifying this expression for general granular materials gives this exponential law:

$$E_c = a(p')^n, \tag{4}$$

with a a constant taking into account the material characteristics and the arrangement of the grains, $n = 2/3$ for glass beads and p' is the mean effective stress defined as [22, 30]:

$$p' = \frac{(\sigma_1 + \sigma_2 + \sigma_3)}{3} = \frac{(\sigma_1 + 2\sigma_3)}{3}. \tag{5}$$

Considering the calculation of the Young modulus E_c at low (negligible) deviatoric stress, the mean effective stress corresponds to the radial stress (confining pressure):

$$p' \approx \frac{(\sigma_3 + 2\sigma_3)}{3} = \sigma_3. \tag{6}$$

Figure 7 illustrates the exponential expression of the Young modulus in compression E_c for the five classes of glass beads (cfr. Table 1). The mean stress has been assumed to be equivalent to the confining pressure varying between $\Delta P = 50.5\,\mathrm{kPa}$ and $\Delta P = 404\,\mathrm{kPa}$. In this case, the

equivalent Young modulus E_c follows an exponential law. The calculation with a 95% confidence of the exponential coefficient gives $n \approx 0.53$ which is relatively close to the theoretical $n = \frac{2}{3}$.

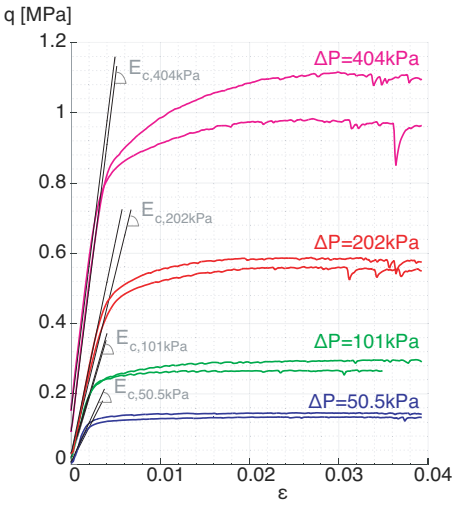

Figure 6: *Stress strain curves for the different confining pressures ΔP. The Young modulus E_c and the ultimate stress q_u are increasing with ΔP.*

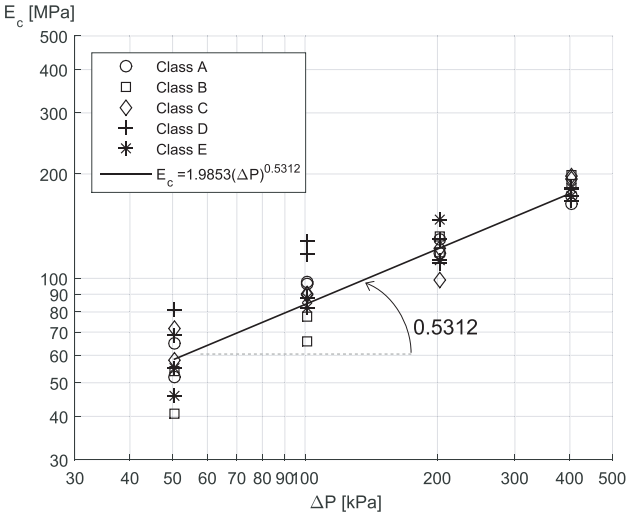

Figure 7: *The logarithmic law of the compression Young modulus E_c is confirmed within the range $\Delta P = 50.5\,\mathrm{kPa} \rightarrow 404\,\mathrm{kPa}$. The exponential law is $E_c = K(\bar{d})p^{0.5312}$. A low dependence on the mean diameter $\bar{d}$ of the glass beads is observed.*

3.2 Three-Point Bending Test

The three-point bending tests are performed for a given pressure difference ΔP obtained from a vacuum pump applying a suction in the specimen. Notice that the maximum theoretical difference of pressure that can be reached by using a vacuum pump is $\Delta P_{max} = P_{atm} \approx 101\,\mathrm{kPa}$ if a high vacuum is reached in the specimen. In the case of the triaxial tests, a larger pressure difference can be reached as the pressure of the environment can be controlled. The initial test is performed at $\Delta P = 70\,\mathrm{kPa}$ and allows for studying the influence of the grain size of the different glass beads. The influence of the specimen diameter D is also studied. Figure 8 shows the force-displacement curves for class C beads (cfr. Table 1) and for the specimen with $D = 15\,\mathrm{mm}$. The procedure used in these tests is similar to the triaxial tests: in order to ensure a good linear behavior and a more repeatable measurement of the equivalent Young modulus in bending E_b, a series of ten loading and unloading cycles are performed. The small hysteresis observed in the zoomed-in Figure 8 (B) between the loading and unloading curves is acceptable as the slope hysteresis is even smaller. The equivalent flexural stiffness is evaluated by Equation 3.

The forces and displacements used in the stiffness calculation correspond to the linear region of the new loading curves (with a 10% margin on the force as in the triaxial compression tests). It has been observed that the repeatability is better for the last loading/unloading cycles. Therefore, the stiffness results are evaluated on the last six cycles out of the ten as they show

a stable result. This choice is motivated by the definition of a procedure that gives repetitive results for bending tests. The ultimate force is not measured in theses tests evaluating the linear behavior only.

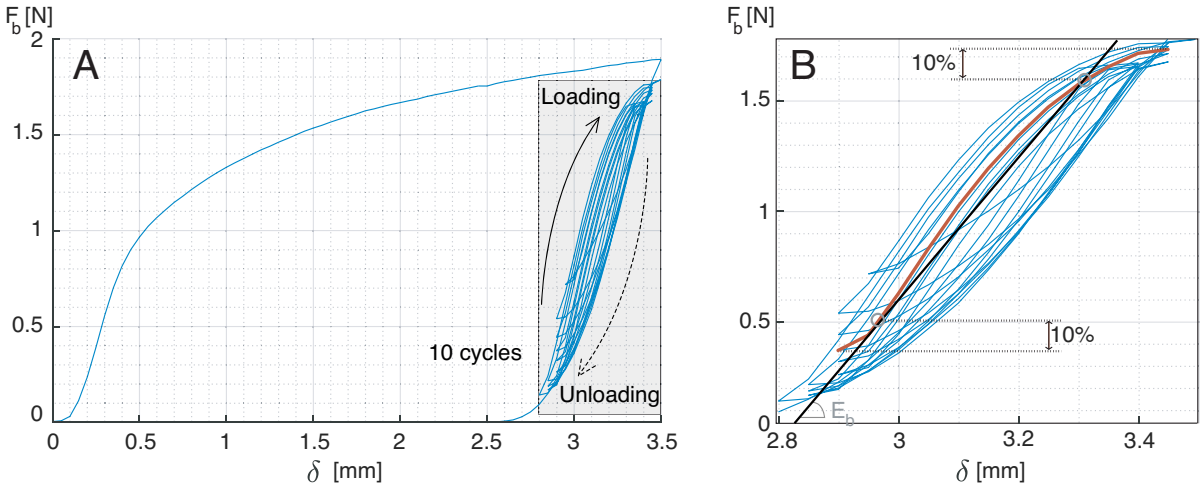

Figure 8: *(A) Force-displacement curves with ten cycles of loading and unloading used to cancel initial conditioning and to improve the measurement of the stiffness of the specimens. (B) Zoomed-in of highlighted data in (A). The slope giving E_b is measured by a linear regression on a specific part of the curve with a 10% margin on the bending force F_b. Small hysteresis is observed during the load and the unload.*

Figure 9a gives the flexural stiffness E_bI and Figure 9b gives the equivalent Young modulus E_b for the different classes of glass beads for the two diameters of the specimens with a pressure difference of $\Delta P = 70\,\mathrm{kPa}$. The eqivalent bending Young modulus E_b is a function of the compression Young modulus E_c and has therefore not the same meaning as this modulus E_c. It appears that the specimens with a lower diameter have a larger equivalent Young modulus in bending E_b. This characteristic should be proper to an equivalent continuous material, but it seems to be dependent on the cross-section of the specimens, unlike it is described in [29]. We can also see from these figures that the class C (cfr. Table 1) of the glass beads seems to be an optimum in terms of flexural stiffness and equivalent Young modulus in bending E_b, as observed in [5].

In order to compare the results of the bending tests with the triaxial tests, a variation on the pressure difference is performed for specimens filled with the optimal class of glass beads (class C, cfr. Table 1). In Figure 10, the equivalent bending Young modulus E_b is compared for several pressure differences. The bending Young modulus E_b is increasing linearly with ΔP for a range of pressure difference $\Delta P = 30 \rightarrow 70\,\mathrm{kPa}$. The gain of stiffness α is given by Equation 7. The calculation of this gain between a rigid state at $\Delta P = 70\,\mathrm{kPa}$ and a flexible state at $\Delta P = 0\,\mathrm{kPa}$ for class C beads gives $\alpha = 46$ and $\alpha = 56$ for tube diameters $D = 15\,\mathrm{mm}$ and $D = 20\,\mathrm{mm}$ respectively.

$$\alpha = \frac{E_{b,rigid}I}{E_{b,flexible}I} = \frac{E_{b,rigid}}{E_{b,flexible}} \tag{7}$$

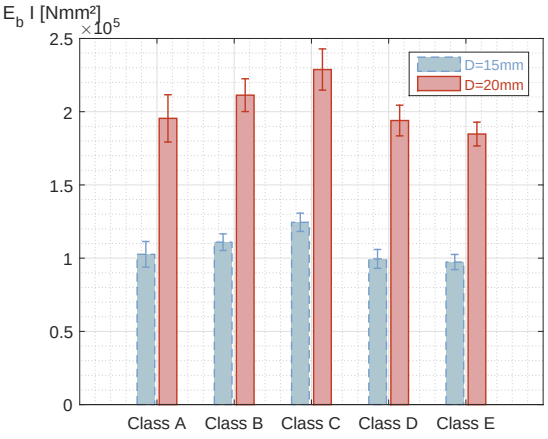

(a) *Flexural stiffness*

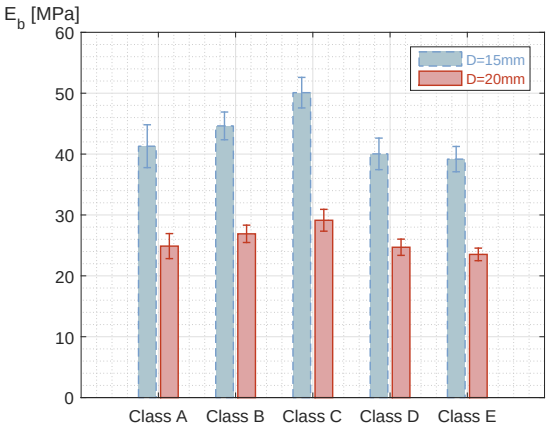

(b) *Equivalent Young modulus in bending*

Figure 9: *The value of the second moment of area has a strong influence on the flexural stiffness, unlike the mean diameter $\bar{d}$ of the glass beads. The specimens with smaller diameter D seem to have an advantage in terms of equivalent Young modulus in bending E_b.*

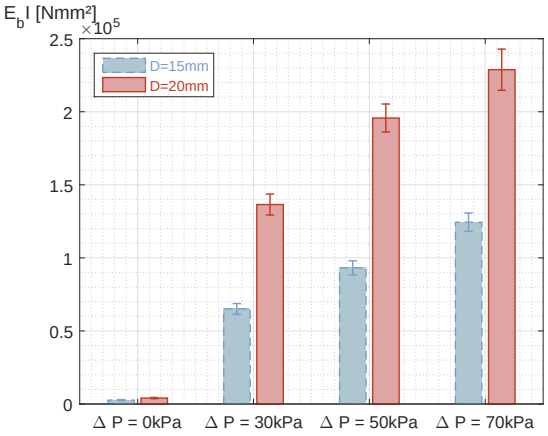

(a) *Flexural stiffness*

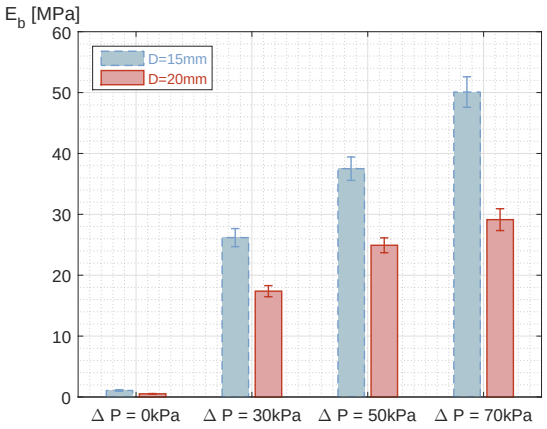

(b) *Equivalent Young modulus in bending*

Figure 10: *The pressure difference influences greatly the flexural stiffness and the equivalent bending Young modulus E_b of the specimens. The smaller diameter D specimens perform better on the bending Young modulus E_b for all pressure differences.*

4 Discussion

In the previous sections, the experimental results of the Granular Jamming solution have been presented and briefly commented. The pressure difference is the main parameter able to tune the stiffness of the specimens. Following an exponential law, the largest stiffness is obtained with the largest pressure difference. In the case of triaxial bending test, a pressure difference larger than the atmospheric pressure can be achieved. In the case of the bending tests, the maximum theoretical pressure difference is equivalent to an atmospheric pressure as a suction is applied in the specimens working in ambient conditions. A linear relation between bending Young modulus and pressure difference has been observed from $30\,\mathrm{kPa}$ to $70\,\mathrm{kPa}$

The size of the micro glass beads has a low influence on the stiffness of the specimens. An

optimum seems to be obtained for class C beads. This optimum is not yet very well understood, but further investigations on this optimum have to be performed in the case of miniaturised specimens.

A model linking the results of the triaxial compression tests and the bending test has to be developed. The exponential law of Young modulus in compression E_c with respect to pressure difference may be extended to Young modulus in bending E_b.

5 Conclusion

The Granular Jamming principle has been used in this study to perform a change of stiffness of tubular-shaped specimens for future medical applications. Their performances have been characterised through different and complementary manners (compression and bending testing). This solution gives good tunable stiffness results by vacuuming the specimen or applying a pressure difference as gain of stiffness of the order of 50 can be obtained for a pressure difference lower than the atmospheric pressure.

The Granular Jamming solution is close to meet the required performances compared to the current range of flexural stiffness of endoscopes on the market. This solution has to be further studied for medical application on the aspects of biocompatibility, safety and miniaturised design. Numerous studies can still be performed to complete the understanding of this solution to the variable stiffness problematic about the various parameters that can be adjusted.

6 Acknowledgements

This work was supported by the F.N.R.S. through a F.R.I.A. grant and a Research Project PDR T1002.14. This project was partially funded by a FER funding provided by the Université Libre de Bruxelles. The authors would like to acknowledge the ARC ULB-UMons (Prediction) funding for support during this research.

References

[1] Sukho Park, Kyoungrae Cha, and Jongoh Park. Development of biomedical microrobot for intravascular therapy. *International Journal of Advanced Robotic Systems*, 7(1):1, 2010.

[2] Isao Kinoshita, Osamu Katoh, Jin Nariyama, Satoru Otsuji, Hitone Tateyama, Tohru Kobayashi, Nobuhiko Shibata, Tadashi Ishihara, and Nakaaki Ohsawa. Coronary angioplasty of chronic total occlusions with bridging collateral vessels: immediate and follow-up outcome from a large single-center experience. *Journal of the American College of Cardiology*, 26(2):409–415, 1995.

[3] Ario Loeve, Paul Breedveld, and Jenny Dankelman. Scopes too flexible... and too stiff. *IEEE pulse*, 1(3):26–41, 2010.

[4] Nadia G Cheng, Maxim B Lobovsky, Steven J Keating, Adam M Setapen, Katy I Gero, Anette E Hosoi, and Karl D Iagnemma. Design and analysis of a robust, low-cost, highly articulated manipulator enabled by jamming of granular media. In *Robotics and Automation (ICRA), 2012 IEEE International Conference on*, pages 4328–4333. IEEE, 2012.

[5] Arjo J Loeve, Oscar S van de Ven, Johan G Vogel, Paul Breedveld, and Jenny Dankelman. Vacuum packed particles as flexible endoscope guides with controllable rigidity. *Granular matter*, 12(6):543–554, 2010.

[6] Matteo Cianchetti, Tommaso Ranzani, Giada Gerboni, Thrishantha Nanayakkara, Kaspar Althoefer, Prokar Dasgupta, and Arianna Menciassi. Soft robotics technologies to address shortcomings in today's minimally invasive surgery: the stiff-flop approach. *Soft Robotics*, 1(2):122–131, 2014.

[7] Allen Jiang, Georgios Xynogalas, Prokar Dasgupta, Kaspar Althoefer, and Thrishantha Nanayakkara. Design of a variable stiffness flexible manipulator with composite granular jamming and membrane coupling. In *Intelligent Robots and Systems (IROS), 2012 IEEE/RSJ International Conference on*, pages 2922–2927. IEEE, 2012.

[8] Allen Jiang, Tommaso Ranzani, Giada Gerboni, Laura Lekstutyte, Kaspar Althoefer, Prokar Dasgupta, and Thrishantha Nanayakkara. Robotic granular jamming: Does the membrane matter? *Soft Robotics*, 1(3):192–201, 2014.

[9] Yong-Jae Kim, Shanbao Cheng, Sangbae Kim, and Karl Iagnemma. A novel layer jamming mechanism with tunable stiffness capability for minimally invasive surgery. *IEEE Transactions on Robotics*, 29(4):1031–1042, 2013.

[10] Siyang Zuo, Kazuo Iijima, Takahiro Tokumiya, and Ken Masamune. Variable stiffness outer sheath with "dragon skin" structure and negative pneumatic shape-locking mechanism. *International journal of computer assisted radiology and surgery*, 9(5):857–865, 2014.

[11] Arjo J Loeve, Dick H Plettenburg, Paul Breedveld, and Jenny Dankelman. Endoscope shaft-rigidity control mechanism:"forguide". *IEEE Transactions on Biomedical Engineering*, 59(2):542–551, 2012.

[12] Yong-Jae Kim, Shanbao Cheng, Sangbae Kim, and Karl Iagnemma. A stiffness-adjustable hyperredundant manipulator using a variable neutral-line mechanism for minimally invasive surgery. *IEEE transactions on robotics*, 30(2):382–395, 2014.

[13] Intelligent material able to adjust itself accordingly to ensure the highest level of comfort & affinity with human body. Technical report, SMP Technologies Inc., 2014.

[14] Izabela K Kuder, Andres F Arrieta, Wolfram E Raither, and Paolo Ermanni. Variable stiffness material and structural concepts for morphing applications. *Progress in Aerospace Sciences*, 63:33–55, 2013.

[15] GD Bell and K Burn. Measurement of the stiffness of endoscopes—a plea for commonality. *Gut*, 49(1):154–154, 2001.

[16] Zeeshan Qaiser, Liping Kang, and Shane Johnson. Design of a bioinspired tunable stiffness robotic foot. *Mechanism and Machine Theory*, 110:1–15, 2017.

[17] Yanqing Liu, Hiroshi Matsuhisa, and Hideo Utsuno. Semi-active vibration isolation system with variable stiffness and damping control. *Journal of sound and vibration*, 313(1):16–28, 2008.

[18] Xingliang Fan, Lu Zhu, Ke Wang, Bingjie Wang, Yaozu Wu, Wei Xie, Chengyu Huang, Barbara Pui Chan, and Yanan Du. Stiffness-controlled thermoresponsive hydrogels for cell harvesting with sustained mechanical memory. *Advanced Healthcare Materials*, 6(5), 2017.

[19] Eric Brown, Nicholas Rodenberg, John Amend, Annan Mozeika, Erik Steltz, Mitchell R Zakin, Hod Lipson, and Heinrich M Jaeger. Universal robotic gripper based on the jamming of granular material. *Proceedings of the National Academy of Sciences*, 107(44):18809–18814, 2010.

[20] Jean-Pierre Bardet. *Experimental soil mechanics*. Prentice Hall Upper Saddle River, NJ, 1997.

[21] Hakan Güneyli and Tolga Rüşen. Effect of length-to-diameter ratio on the unconfined compressive strength of cohesive soil specimens. *Bulletin of Engineering Geology and the Environment*, 75(2):793–806, 2016.

[22] R Nova and David Muir Wood. A constitutive model for sand in triaxial compression. *International Journal for Numerical and Analytical Methods in Geomechanics*, 3(3):255–278, 1979.

[23] Nadia G Cheng. *Design and analysis of jammable granular systems*. PhD thesis, Massachusetts Institute of Technology, 2013.

[24] David Hellier, Faris Albermani, Brendon Evans, Hans De Visser, Clayton Adam, and Josh Passenger. Flexural and torsional rigidity of colonoscopes at room and body temperatures. *Proceedings of the Institution of Mechanical Engineers, Part H: Journal of Engineering in Medicine*, 225(4):389–399, 2011.

[25] José João de Espíndola, Silva Neto, et al. Identification of flexural stiffness parameters of beams. *Journal of the Brazilian Society of Mechanical Sciences*, 23(4):217–225, 2001.

[26] CEN. Plastics—determination of flexural properties (iso 178 : 2001), February 2003. EN ISO 178 : 2003 E.

[27] Matthew Kroh and Kevin M Reavis. *The SAGES Manual Operating Through the Endoscope*. Springer, 2016.

[28] Athanasios G Athanassiadis, Marc Z Miskin, Paul Kaplan, Nicholas Rodenberg, Seung Hwan Lee, Jason Merritt, Eric Brown, John Amend, Hod Lipson, and Heinrich M Jaeger. Particle shape effects on the stress response of granular packings. *Soft Matter*, 10(1):48–59, 2014.

[29] PY Hicher and A Rahma. Micro-macro correlations for granular media. application to the modelling of sands. *European Journal of Mechanics Series - A/Solids*, 13:763–763, 1994.

[30] Pierre-Yves Hicher. Elastic properties of soils. *Journal of Geotechnical Engineering*, 122(8):641–648, 1996.